Journal of Sound and Vibration (2002) **251**(2), 329–348
doi:10.1006/jsvi.2001.3993, available online at http://www.idealibrary.com on IDEAL®

GENERALIZED DIFFERENTIAL QUADRATURE METHOD FOR THE FREE VIBRATION OF TRUNCATED CONICAL PANELS

K. Y. Lam, H. Li, T. Y. Ng and C. F. Chua

Institute of High Performance Computing, National University of Singapore, 89C Science Park Drive, #02-11/12, The Rutherford, Singapore Science Park 1, 118261 *Singapore. E-mail: ngty@ihpc.nus.edu.sg*

(*Received* 8 *May* 2001, *and in final form* 5 *September* 2001)

This paper presents an improved generalized differential quadrature (GDQ) method for the investigation of the effects of boundary conditions on the free vibration characteristics of truncated conical panels. The truncated conical panel is an important geometrical shape in the fields of aerospace, marine and structural engineering. However, despite this importance, few works in free vibration analysis have dealt with this particular geometry. In this work, the vibration characteristics of clamped and simply supported truncated conical shells are obtained for various circumferential wave numbers. Further, the effects of the vertex and subtended angles on the frequency parameters are also examined in detail. Due to limited published results in the open literature, results for a range of cases are compared with those generated from the commercial finite element solver McNeal–Schwendler Corporation Nastran, and excellent agreement is observed.

1. INTRODUCTION

Truncated conical shell panels have a wide range of engineering applications, particularly in aerospace, marine and structural engineering. Many structures comprise at least a few components with this geometrical profile, such as turbine blades or aircraft fuselages. In practice, such components can be subjected to varying levels of dynamic stresses. A reliable way to predict the behavior of such components is essential for the sound and reliable design of this class of structural components. In a review by Chang [1], there was no reference dealing directly with the free vibration of such truncated conical panels. The proposed reason was the difficulties involved in such an open structure. When dealing with a completely closed conical shell, the 2-D problem can be reduced using standard Fourier decomposition. For a conical panel, however, it is not possible to perform such a reduction operation, and the two-dimensional field must be dealt with directly. In contrast, much work has been done on the analyses of closed truncated conical shells. A few of the notable works include Saunders *et al.* [2], Goldberg *et al.* [3], Kalnins [4], Garnet and Kemper [5], Siu and Bert [6], Irie *et al.* [7, 8], Tong [9, 10], Shu [11] and Wang *et al.* [12].

For the case of conical panels, an early work by Rossetos and Parisse [13] examined their dynamic responses. Ashwell and Gallagher [14, 15] approached this subject using the finite elemental approach. However, additional elements with large degrees of freedom had to be used to ensure the continuity and equilibrium between the elements in their model. Approximations for the fundamental frequencies and buckling loads were presented by Teichmann [16] for conical shell panels under initial stress. Srinivasan and Krishnan [17] used the simple Donnell's shell theory and an integral equation method to derive the

0022-460X/02/120329 + 20 $35.00/0

natural frequencies and vibration mode of clamped isotropic conical panel. However, it was noted by Cheung *et al.* [18] that the results presented in the article of Srinivasan and Krishnan's [17] have yet to converge. Cheung *et al.* [18] developed and demonstrated the validity of the spline finite strip method for the analysis of the vibration characteristics of various singly curved shell structures such as circular arches, clamped conical shells and elliptical shells. An approach based on spline approximation was presented by Grigorenko *et al.* [19] for the static analysis of thin conical panels. Liew and Lim [20] modelled shallow conical shell panels using the Rayleigh–Ritz method. This was extended to include first order shear deformation in Lim and Liew [21]. Lim and Kitipornchai [22] have also analyzed this problem by adopting a natural conical co-ordinate system such that any approximations in geometry will be eliminated. Bardell *et al.* [23] used the h–p finite-element method together with Love's thin shell equations to investigate the natural frequencies of conical sandwich panels.

Although the vibration of conical panels can be easily solved using commercial finite-element packages, these commercial packages are unable to handle other classes of dynamic problems such as parametric resonance or even the vibration characteristics of rotating panels. The present development of the GDQ formulation for solving the vibration of conical panels establishes the differential quadrature framework for solving these more complicated dynamic problems. A further advantage of the GDQ over finite element method (FEM) is the computational efficiency. In the FEM, the weak forms must first be generated from the governing differential equations of motion. Following this, numerical approximations such as Gaussian integration are then employed to transforms the integral weak forms to the algebraic form for the elemental stiffness and masses, before assembling them to form the corresponding global matrices. In the GDQ method, however, the governing differential equations of motion are directly transformed in one step to obtain the final algebraic forms. The method of differential quadrature has been widely used for a variety of problems, see Gutierrez *et al.* [24] and the review article by Bert and Malik [25]. To the authors' knowledge, the generalized differential quadrature (GDQ) method has not been applied to the free vibration of conical shell panels. Further, no attention has been given in previous frequency studies on this geometry to the effects of different boundary conditions. This paper will demonstrate the feasibility and effectiveness of the GDQ method for thin isotropic conical shell panels, and in the process, look into the effects of vertex and subtended angles on the natural frequencies. These effects will be examined under four different boundary condition types.

2. GOVERNING EQUATIONS AND DISPLACEMENT FIELD

Consider a homogeneous, isotropic, thin conical shell panel as shown in Figure 1, where the half vertex angle is denoted by α, the subtended angle by β, the thickness by h and the slanted length of the shell by L. The symbols a and b represent the radii of the smaller and larger ends of the conical shell respectively. The radius at any one point of the shell can be calculated by the simple relationship $r(x) = a + x\sin\alpha$. The middle surface between the thickness of the shell will be taken as the reference surface for our ground-based orthogonal co-ordinate system (x, θ, z). The components of displacement in the meridional, x, circumferential, θ, and normal, z, directions are denoted by u, v and w respectively.

The governing equations of motion in terms of the displacements and force and moment resultants for the free vibration of a conical shell can be written as follows, see Lam and Li [26]:

$$\frac{\partial N_x}{\partial x} + \frac{1}{r(x)}\frac{\partial N_{x\theta}}{\partial \theta} + \frac{\sin\alpha}{r(x)}(N_x - N_\theta) - \rho h\frac{\partial^2 u}{\partial t^2} = 0, \tag{1}$$

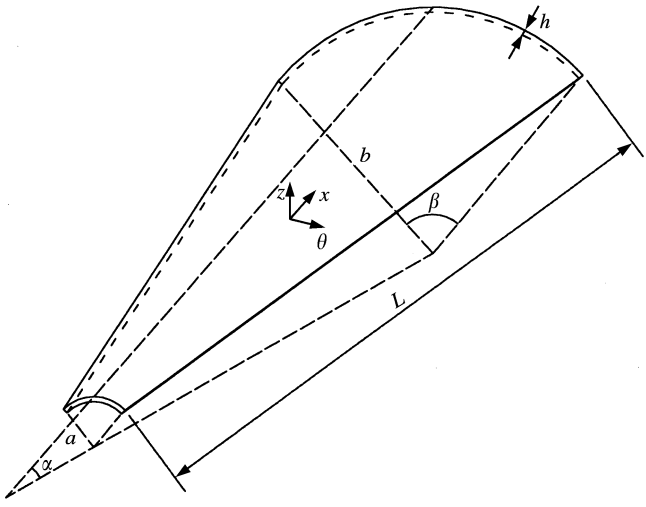

Figure 1. Geometry of the truncated conical panel.

$$\frac{\partial N_{x\theta}}{\partial x} + \frac{1}{r(x)}\frac{\partial N_\theta}{\partial \theta} + \frac{\cos\alpha}{r(x)}\frac{\partial M_{x\theta}}{\partial x} + \frac{\cos\alpha}{r^2(x)}\frac{\partial M_\theta}{\partial \theta} + 2\frac{\sin\alpha}{r(x)}N_{x\theta} - \rho h\frac{\partial^2 v}{\partial t^2} = 0, \tag{2}$$

$$\frac{\partial^2 M_x}{\partial x^2} + \frac{2}{r(x)}\frac{\partial^2 M_{x\theta}}{\partial x \partial \theta} + \frac{1}{r^2(x)}\frac{\partial^2 M_\theta}{\partial \theta^2} + \frac{2\sin\alpha}{r(x)}\frac{\partial M_x}{\partial x} - \frac{\sin\alpha}{r(x)}\frac{\partial M_\theta}{\partial x} - \frac{\cos\alpha}{r(x)}N_\theta - \rho h\frac{\partial^2 w}{\partial t^2} = 0, \tag{3}$$

where

$$\rho = \rho(x, \theta) = \frac{1}{h}\int_{-h/2}^{h/2} \rho^*(x, \theta, z)\,\mathrm{d}z, \tag{4}$$

$$r(x) = a + x\sin\alpha, \tag{5}$$

where $\rho^*(x, \theta, z)$ is the density of the conical shell and $\rho(x, \theta)$ the average density in the normal z direction. $\mathbf{N}^{\mathrm{T}} = \{N_x, N_\theta, N_{x\theta}\}$ and $\mathbf{M}^{\mathrm{T}} = \{M_x, M_\theta, M_{x\theta}\}$ are the force and moment resultants defined by the following constitutive equations:

$$\begin{Bmatrix}\mathbf{N}\\ \mathbf{M}\end{Bmatrix} = \begin{Bmatrix} N_x \\ N_\theta \\ N_{x\theta} \\ M_x \\ M_\theta \\ M_{x\theta}\end{Bmatrix} = \begin{bmatrix}[A_{ij}]_{3\times 3} & [B_{ij}]_{3\times 3} \\ [B_{ij}]_{3\times 3} & [D_{ij}]_{3\times 3}\end{bmatrix}\begin{Bmatrix} e_1 \\ e_2 \\ e_{12} \\ \kappa_1 \\ \kappa_2 \\ \kappa_{12}\end{Bmatrix} = \begin{bmatrix}\mathbf{A} & \mathbf{B} \\ \mathbf{B} & \mathbf{D}\end{bmatrix}\begin{Bmatrix}\mathbf{e}\\ \mathbf{k}\end{Bmatrix}, \tag{6}$$

where $\mathbf{e}^{\mathrm{T}} = \{e_1, e_2, e_{12}\}$ and $\mathbf{k}^{\mathrm{T}} = \{\kappa_1, \kappa_2, \kappa_{12}\}$ are the reference surface strains and curvatures. The subscripts "1" and "2" denote the meridional and circumferential directions. These strain and curvature components can be given by the following geometric

deformation relationships of the reference surface for a conical shell as

$$e_1 = \frac{\partial u}{\partial x}, \qquad e_2 = \frac{1}{r(x)}\frac{\partial v}{\partial \theta} + \frac{u\sin\alpha + w\cos\alpha}{r(x)}, \qquad \kappa_1 = -\frac{\partial^2 w}{\partial x^2},$$

$$\kappa_2 = -\frac{1}{r^2(x)}\frac{\partial^2 w}{\partial \theta^2} + \frac{\cos\alpha}{r^2(x)}\frac{\partial v}{\partial \theta} - \frac{\sin\alpha}{r(x)}\frac{\partial w}{\partial x}, \tag{7}$$

$$e_{12} = \frac{1}{r(x)}\frac{\partial u}{\partial \theta} + \frac{\partial v}{\partial x} - \frac{v\sin\alpha}{r(x)}, \quad \kappa_{12} = 2\left(-\frac{1}{r(x)}\frac{\partial^2 w}{\partial x \partial \theta} + \frac{\sin\alpha}{r^2(x)}\frac{\partial w}{\partial \theta} + \frac{\cos\alpha}{r(x)}\frac{\partial v}{\partial x} - \frac{v\sin\alpha\cos\alpha}{r^2(x)}\right).$$

Based on the hypothesis of Love's [27] first approximation which states that the strain components, e_x, e_ϑ and $e_{x\theta}$, at any point of a conical shell can be expressed by a linear function of the normal co-ordinate z in terms of the reference strains and curvatures, each of these components may be expressed as

$$e_x = e_1 + z\kappa_1, \qquad e_\theta = e_2 + z\kappa_2, \qquad e_{x\theta} = e_{12} + z\kappa_{12}. \tag{8}$$

In the constitutive equation, equation (6), $\mathbf{A} = [A_{ij}]_{3\times 3}$, $\mathbf{B} = [B_{ij}]_{3\times 3}$ and $\mathbf{D} = [D_{ij}]_{3\times 3}$ are the extensional, coupling and bending stiffnesses, respectively, for the isotropic conical shell and can be written as

$$\mathbf{A} = [A_{ij}]_{3\times 3} = \frac{Eh}{(1-\mu^2)}\begin{bmatrix} 1 & \mu & 0 \\ \mu & 1 & 0 \\ 0 & 0 & \dfrac{1-\mu}{2} \end{bmatrix},$$

$$\mathbf{B} = [B_{ij}]_{3\times 3} = 0, \tag{9}$$

$$\mathbf{D} = [D_{ij}]_{3\times 3} = \frac{Eh^3}{12(1-\mu^2)}\begin{bmatrix} 1 & \mu & 0 \\ \mu & 1 & 0 \\ 0 & 0 & 1-\mu \end{bmatrix}.$$

Substituting equations (6) and (7) into the governing equations of motion, equations (1)–(3), yields

$$\begin{aligned} L_{11}u + L_{12}v + L_{13}w &= 0, \\ L_{21}u + L_{22}v + L_{23}w &= 0, \\ L_{31}u + L_{32}v + L_{33}w &= 0, \end{aligned} \tag{10}$$

where L_{ij} are the differential operators given by

$$L_{11} = -\rho h\frac{\partial^2}{\partial t^2} - \frac{A_{22}\sin^2\alpha}{r^2(x)} + \frac{A_{66}}{r^2(x)}\frac{\partial^2}{\partial \theta^2} + \frac{A_{11}\sin\alpha}{r(x)}\frac{\partial}{\partial x} + A_{11}\frac{\partial^2}{\partial x^2}, \tag{11}$$

$$L_{12} = -\frac{(A_{22} + A_{66})\sin\alpha}{r^2(x)}\frac{\partial}{\partial\theta} + \frac{(A_{12} + A_{66})}{r(x)}\frac{\partial^2}{\partial x\partial\theta}, \tag{12}$$

$$L_{13} = -\frac{A_{22}\cos\alpha\sin\alpha}{r^2(x)} + \frac{A_{12}\cos\alpha}{r(x)}\frac{\partial}{\partial x}, \tag{13}$$

$$L_{21} = \frac{(A_{22} + A_{66})\sin\alpha}{r^2(x)}\frac{\partial}{\partial\theta} + \frac{(A_{12} + A_{66})}{r(x)}\frac{\partial^2}{\partial x\partial\theta}, \tag{14}$$

$$\begin{aligned} L_{22} = &-\rho h\frac{\partial^2}{\partial t^2} + \frac{4D_{66}\cos^2\alpha\sin^2\alpha}{r^4(x)} - \frac{A_{66}\sin^2\alpha}{r^2(x)} + \left(\frac{D_{22}\cos^2\alpha}{r^4(x)} + \frac{A_{22}}{r^2(x)}\right)\frac{\partial^2}{\partial\theta^2} \\ &-\left(\frac{4D_{66}\cos^2\alpha\sin\alpha}{r^3(x)} - \frac{A_{66}\sin\alpha}{r(x)}\right)\frac{\partial}{\partial x} + \left(\frac{2D_{66}\cos^2\alpha}{r^2(x)} + A_{66}\right)\frac{\partial^2}{\partial x^2}, \end{aligned} \tag{15}$$

$$\begin{aligned} L_{23} = &-\left(\frac{4D_{66}\cos\alpha\sin^2\alpha}{r^4(x)} - \frac{A_{22}\cos\alpha}{r^2(x)}\right)\frac{\partial}{\partial\theta} - \frac{D_{22}\cos\alpha}{r^4(x)}\frac{\partial^3}{\partial\theta^3} \\ &-\frac{(D_{22} - 4D_{66})\cos\alpha\sin\alpha}{r^3(x)}\frac{\partial^2}{\partial x\partial\theta} - \frac{(D_{12} + 2D_{66})\cos\alpha}{r^2(x)}\frac{\partial^3}{\partial x^2\partial\theta}, \end{aligned} \tag{16}$$

$$L_{31} = -\frac{A_{22}\cos\alpha\sin\alpha}{r^2(x)} - \frac{A_{12}\cos\alpha}{r(x)}\frac{\partial}{\partial x}, \tag{17}$$

$$\begin{aligned} L_{32} = &\frac{D_{22}\cos\alpha}{r^4(x)}\frac{\partial^3}{\partial\theta^3} + \left(\frac{2(D_{12} + D_{22} + 4D_{66})\cos\alpha\sin^2\alpha}{r^4(x)} - \frac{A_{22}\cos\alpha}{r^2(x)}\right)\frac{\partial}{\partial\theta} \\ &-\frac{(2D_{12} + D_{22} + 8D_{66})\cos\alpha\sin\alpha}{r^3(x)}\frac{\partial^2}{\partial x\partial\theta} + \frac{(D_{12} + 2D_{66})\cos\alpha}{r^2(x)}\frac{\partial^3}{\partial x^2\partial\theta}, \end{aligned} \tag{18}$$

$$\begin{aligned} L_{33} = &-\rho h\frac{\partial^2}{\partial t^2} - \frac{A_{22}\cos^2\alpha}{r^2(x)} - \frac{D_{22}}{r^4(x)}\frac{\partial^4}{\partial\theta^4} - \frac{2(D_{12} + D_{22} + 4D_{66})\sin^2\alpha}{r^4(x)}\frac{\partial^2}{\partial\theta^2} \\ &-\frac{D_{22}\sin^3\alpha}{r^3(x)}\frac{\partial}{\partial x} + \frac{2(D_{12} + 4D_{66})\sin\alpha}{r^3(x)}\frac{\partial^3}{\partial x\partial\theta^2} + \frac{D_{22}\sin^2\alpha}{r^2(x)}\frac{\partial^2}{\partial x^2} \\ &-\frac{(2D_{12} - 4D_{66})}{r^2(x)}\frac{\partial^4}{\partial x^2\partial\theta^2} - \frac{2D_{11}\sin\alpha}{r(x)}\frac{\partial^3}{\partial x^3} - D_{11}\frac{\partial^4}{\partial x^4}. \end{aligned} \tag{19}$$

The governing partial differential equations, equations (1)–(3), do not take into account the boundary conditions at any of the edges. Thus, the formulation is general to this stage with regard to edge boundary conditions. In this present work, simply supported boundary conditions are assumed at both the straight edges of the conical panel for all present numerical computations, i.e.,

$$u = 0, \quad w = 0, \quad N_\theta = 0, \quad M_\theta = 0 \quad \text{at} \quad \theta = 0, \beta. \tag{20}$$

For the curved edges, $x = 0$ and L, simply supported boundary conditions are expressed as

$$v = 0, \quad w = 0, \quad N_x = 0, \quad M_x = 0 \quad \text{at} \quad x = 0 \text{ or } L \tag{21}$$

and for clamped boundary conditions

$$u = 0, \quad v = 0, \quad w = 0, \quad \frac{\partial w}{\partial x} = 0 \quad \text{at} \quad x = 0 \text{ or } L. \tag{22}$$

To satisfy the simply supported boundary condition at the straight edges, the displacement field can be simulated by the following trial functions:

$$\begin{aligned}\mathbf{U}^{\mathrm{T}} &= \{u(x, \theta, t) \quad v(x, \theta, t) \quad w(x, \theta, t)\} \\ &= \left\{U(x)\sin\left(\frac{n\pi\theta}{\beta}\right)\mathrm{e}^{\mathrm{i}\omega t} \quad V(x)\cos\left(\frac{n\pi\theta}{\beta}\right)\mathrm{e}^{\mathrm{i}\omega t} \quad W(x)\sin\left(\frac{n\pi\theta}{\beta}\right)\mathrm{e}^{\mathrm{i}\omega t}\right\}.\end{aligned} \tag{23}$$

We substitute the trial functions, equation (23), into the displacement governing equations, equation (10), and the terms with θ and t will be eliminated and the governing equation would be simplified as follows:

$$\begin{aligned}&J_{110}U + J_{111}U^{(1)} + J_{112}U^{(2)} + J_{120}V + J_{121}V^{(1)} + J_{122}V^{(2)} + J_{130}W \\ &\quad + J_{131}W^{(1)} + J_{132}W^{(2)} = 0, \\ &J_{210}U + J_{211}U^{(1)} + J_{212}U^{(2)} + J_{220}V + J_{221}V^{(1)} + J_{222}V^{(2)} + J_{230}W \\ &\quad + J_{231}W^{(1)} + J_{232}W^{(2)} = 0, \\ &J_{310}U + J_{311}U^{(1)} + J_{312}U^{(2)} + J_{320}V + J_{321}V^{(1)} + J_{322}V^{(2)} + J_{330}W \\ &\quad + J_{331}W^{(1)} + J_{332}W^{(2)} + J_{333}W^{(3)} + J_{334}W^{(4)} = 0\end{aligned} \tag{24}$$

and in matrix form

$$\mathbf{J}\mathbf{U}^* = 0, \tag{25}$$

where $\mathbf{U}^* = \{U(x), V(x), W(x)\}^{\mathrm{T}}$ is an unknown spatial function vector of the mode shape in the meridional x direction. The resulting partial differential operators $\mathbf{J} = [J_{ijk}]$ are listed below:

$$J_{110} = \rho h\omega^2 - \frac{A_{22}\sin^2\alpha + \mathrm{A}_{66}(n\pi/\beta)^2}{r^2(x)}, \qquad J_{111} = \frac{A_{11}\sin\alpha}{r(x)}, \tag{26, 27}$$

$$J_{112} = A_{11}, \qquad J_{120} = \frac{(A_{22} + A_{66})\sin\alpha}{r^2(x)}\left(\frac{n\pi}{\beta}\right), \tag{28, 29}$$

$$J_{121} = -\frac{(A_{12} + A_{66})}{r(x)}\left(\frac{n\pi}{\beta}\right), \qquad J_{122} = 0, \tag{30, 31}$$

$$J_{130} = -\frac{A_{22}\cos\alpha\sin\alpha}{r^2(x)}, \qquad J_{131} = \frac{A_{12}\cos\alpha}{r(x)}, \tag{32, 33}$$

$$J_{132} = 0, \qquad J_{210} = \frac{(A_{22} + A_{66})\sin\alpha}{r^2(x)}\left(\frac{n\pi}{\beta}\right), \tag{34, 35}$$

$$J_{211} = \frac{(A_{12} + A_{66})}{r(x)}\left(\frac{n\pi}{\beta}\right), \qquad J_{212} = 0, \tag{36, 37}$$

$$J_{220} = \rho h\omega^2 + \frac{4D_{66}\cos^2\alpha\sin^2\alpha}{r^4(x)} - \frac{A_{66}\sin^2\alpha}{r^2(x)} - \left(\frac{D_{22}\cos^2\alpha}{r^4(x)} + \frac{A_{22}}{r^2(x)}\right)\left(\frac{n\pi}{\beta}\right)^2, \tag{38}$$

$$J_{221} = -\frac{4D_{66}\cos^2\alpha\sin\alpha}{r^3(x)} + \frac{A_{66}\sin\alpha}{r(x)}, \tag{39}$$

$$J_{222} = \frac{2D_{66}\cos^2\alpha}{r^2(x)} + A_{66}, \tag{40}$$

$$J_{230} = -\left(\frac{4D_{66}\cos\alpha\sin^2\alpha}{r^4(x)} - \frac{A_{22}\cos\alpha}{r^2(x)}\right)\frac{n\pi}{\beta} + \frac{D_{22}\cos\alpha}{r^4(x)}\left(\frac{n\pi}{\beta}\right)^3, \tag{41}$$

$$J_{231} = -\frac{(D_{22} - 4D_{66})\cos\alpha\sin\alpha}{r^3(x)}\left(\frac{n\pi}{\beta}\right), \tag{42}$$

$$J_{232} = -\frac{(D_{12} + 2D_{66})\cos\alpha}{r^2(x)}\left(\frac{n\pi}{\beta}\right), \tag{43}$$

$$J_{310} = -\frac{A_{22}\cos\alpha\sin\alpha}{r^2(x)}, \qquad J_{311} = -\frac{A_{12}\cos\alpha}{r(x)}, \qquad J_{312} = 0, \tag{44–46}$$

$$J_{320} = \frac{D_{22}\cos\alpha}{r^4(x)}\left(\frac{n\pi}{\beta}\right)^3 - \left(\frac{2(D_{12} + D_{22} + 4D_{66})\cos\alpha\sin^2\alpha}{r^4(x)} - \frac{A_{22}\cos\alpha}{r^2(x)}\right)\left(\frac{n\pi}{\beta}\right), \tag{47}$$

$$J_{321} = \frac{(2D_{12} + D_{22} + 8D_{66})\cos\alpha\sin\alpha}{r^3(x)}\left(\frac{n\pi}{\beta}\right), \tag{48}$$

$$J_{322} = -\frac{(D_{12} + 4D_{66})\cos\alpha}{r^2(x)}\left(\frac{n\pi}{\beta}\right), \tag{49}$$

$$J_{330} = \rho h\omega^2 - \frac{A_{22}\cos^2\alpha}{r^2(x)} - \frac{D_{22}}{r^4(x)}\left(\frac{n\pi}{\beta}\right)^4 + \frac{2(D_{12} + D_{22} + 4D_{66})\sin^2\alpha}{r^4(x)}\left(\frac{n\pi}{\beta}\right)^2, \quad (50)$$

$$J_{331} = -\frac{D_{22}\sin^3\alpha}{r^3(x)} - \frac{2(D_{12} + 4D_{66})\sin\alpha}{r^3(x)}\left(\frac{n\pi}{\beta}\right)^2, \quad (51)$$

$$J_{332} = \frac{D_{22}\sin^2\alpha}{r^3(x)} + \frac{(2D_{12} + 4D_{66})}{r^2(x)}\left(\frac{n\pi}{\beta}\right)^2, \quad (52)$$

$$J_{333} = -\frac{2D_{11}\sin\alpha}{r(x)}, \qquad J_{334} = -D_{11}. \quad (53, 54)$$

Expressed in such a form as the above, the generalized differential quadrature method can be easily applied to terms of the same order of derivative in the governing equations of motion.

3. GENERALIZED DIFFERENTIAL QUADRATURE (GDQ) METHOD

The generalized differential quadrature or GDQ method states that the derivatives of a sufficiently smooth function with respect to a co-ordinate direction at a discrete grid point can be approximated by a weighted linear sum of functional values of all the discrete mesh points in that co-ordinate direction. It is based on the analyses of a higher order polynomial approximation in linear vector space to arrive at the weighting coefficient required by the method. The mathematical expression of this basic theorem is expressed as

$$f^{(m)}(x)|_{x=x_i} = \sum_{j=1}^{N} C_{ij}^m f(x_j), \quad (55)$$

where C_{ij}^m are the weighting coefficients.

The difference between the GDQ method and the traditional DQ method is in the way the base polynomials are chosen. As the GDQ method utilizes the Lagrange interpolation polynomial as the base polynomial, it is superior to the DQ method because it allows for greater flexibility in the selection of the location of the grid points. As a result, for the GDQ method, the base polynomial is presented by the Lagrange interpolation polynomial where

$$p_k(x) = M(x)/(x - x_k)M^{(1)}(x_k), \quad (56)$$

$$M(x) = (x - x_1)(x - x_2)(x - x_3)\cdots(x - x_N), \quad (57)$$

$$M^{(1)}(x_k) = (x_k - x_1)(x_k - x_2)\cdots(x_k - x_{k-1})(x_k - x_{k+1})\cdots(x_k - x_{N-1})(x_k - x_N), \quad (58)$$

where $x_1, x_2, x_3, \ldots, x_N$ are the arbitrary co-ordinates of the grid points. When $i \neq j$, the weighting coefficient for first order derivatives, $m = 1$, in equation (55), can be obtained as follows:

$$C_{ij}^1 = M^{(1)}(x_i)/((x_i - x_j)M^{(1)}(x_j)) \quad \text{where } j \neq i \quad \text{and} \quad i = 1, 2, \ldots, N \quad (59)$$

and for the higher order derivatives, $m \geqslant 2$,

$$C_{ij}^m = m(C_{ij}^1 \times C_{ii}^{m-1} - C_{ij}^{m-1}/(x_i - x_j)) \quad \text{for } j \neq i, \quad i, j = 1, 2, \ldots, N,\ m = 2, 3, \ldots, N-1, \tag{60}$$

where N is the total number of grid points. For the terms where $i = j$, C_{ii}^m for all order of derivatives can be obtained from the condition

$$\sum_{j=1}^{N} C_{ij}^m = 0. \tag{61}$$

The reason for this is that any one set of base polynomials can be distinctively mapped by another base polynomial, as stated by the theory of linear vector space. Thus, the unknown function $f(x, t)$ in equation (55) can be approximated by x^k. Then, by assigning a value of 0 to the arbitrary power variable k, equation (55) becomes $\sum_{j=1}^{N} C_{ij}^m = 0$. Using this condition, the values of C_{ii}^m can be easily derived from the other values of C_{ij}^m from equations (59) and (60). One of the advantages of the GDQ method is that it does not impose any constraints on the co-ordinate distribution of the grid points. In this study, we choose to use the cosine grid point distribution in our computations:

$$x_i = (1 - \cos((\mathrm{i} - 1)\pi/(N - 1)))L/2. \tag{62}$$

Substituting equation (55) into the set of reduced governing equations, equation (24), we transform the governing equations in the differential form into a set of linear discrete algebraic equations

$$\mathbf{J}\mathbf{U}^*|_{x=x_i} = \mathbf{C}^*_{3\times 11}\mathbf{U}^{**}_{11\times 1}|_{x=x_i} = 0 \quad (i = 1, 2, 3, \ldots, N), \tag{63}$$

where N is the number of total discrete grid points including the points at both edges in the meridional x direction; $\mathbf{C}^*$ is the 3×11 variable coefficient matrix related to discrete grid point $x = x_i$; $\mathbf{U}^{**}$ is a 11 order column vector and can be written as

$$\begin{aligned}\mathbf{U}^{**\mathrm{T}}|_{x=x_i} = \{&U(x_i),\ U^{(1)}(x_i),\ U^{(2)}(x_i),\ V(x_i),\ V^{(1)}(x_i),\ V^{(2)}(x_i),\\ &W(x_i),\ W^{(1)}(x_i),\ W^{(2)}(x_i),\ W^{(3)}(x_i),\ W^{(4)}(x_i),\end{aligned} \tag{64}$$

$$U^{(m)}(x_i) = \sum_{j=1}^{N} C_{ij}^m U(x_j), \quad V^{(m)}(x_i) = \sum_{j=1}^{N} C_{ij}^m V(x_j), \quad W^{(m)}(x_i) = \sum_{j=1}^{N} C_{ij}^m W(x_j). \tag{65}$$

For a given boundary condition at the curved edges, imposing equation (63) at every discrete point ($i = 1, 2, \ldots, N$) and then rearranging the resulting equation in terms of the natural frequency, ω, we obtained the governing eigenvalue equation in matrix form

$$[\mathbf{R}_{N^*\times N^*} - \omega^2 \mathbf{I}_{N^*\times N^*}]\mathbf{d}_{N^*\times 1} = 0, \tag{66}$$

where $\mathbf{I}$ is a unit matrix, $\mathbf{R}$ is an $N^* \times N^*$ ($N^* = 3 \times N - 8$) characteristic matrix and $\mathbf{d}$ is the N^* order column vector

$$\begin{aligned}\mathbf{d}^{\mathrm{T}} = \{&U(x_2), U(x_3), \ldots, U(x_{N-2}), U(x_{N-1}),\ V(x_2), V(x_3), \ldots, V(x_{N-2}), V(x_{N-1}),\\ &W(x_3), W(x_4), \ldots, W(x_{N-3}), W(x_{N-2})\}.\end{aligned} \tag{67}$$

Using equation (66) for the present conical shell panel, we can compute the natural frequencies for any given combination of geometrical parameters and the material properties.

4. RESULTS AND DISCUSSION

4.1. CONVERGENCE AND COMPARISON STUDIES

In the present study, four boundary condition types are considered, namely: clamped–clamped (C_S–C_L), simply supported–clamped (S_S–C_L), clamped–simply supported (C_S–S_L), and simply supported–simply supported (S_S–S_L). The first alphabet in the acronyms denotes the boundary condition, while the subscript denotes the side in which the boundary condition is applicable. The subscript "S" denotes the edge with the smaller radius, while the subscript "L" denotes the edge with the larger radius. To facilitate comparison of data, all frequency parameter results presented in this section are in the dimensionless form, $f = \omega b(\rho h/A_{11})^{1/2}$.

To ensure convergence of the present results, a detailed study was conducted in which the convergence characteristics were observed. Also, comparison studies against results generated by the commercial finite element solver MSC/Nastran using eight-noded shell elements were conducted. For these FEM results, well-converged results were obtained using a 200×40 grid size or 8000 elements. The tabulated results of these convergence and comparison studies are presented in Tables 1–3 for a range of parametric cases. For all four cases of boundary conditions considered here, as the number of grid points is increased, monotonic convergence is observed. It is found that the use of 15 grid points produced sufficiently converged results with generally less than 1% difference when compared with results using 13 grid points. All subsequent results in the following parametric studies are thus obtained using 15 grid points. It is also observed that the present GDQ results agree very well with the FEM results for all four boundary condition cases with less than 4% difference between the two sets of results. To provide a feel for some of the frequency results, the fundamental mode $(m, n) = (1, 2)$ of a clamped C_S–C_L panel of shell parameters $a = 3\,\text{cm}$, $L = 20a$, $h = 0{\cdot}015a$, $\alpha = 20^\circ$ and $\beta = 60^\circ$, with material properties $E = 7{\cdot}0 \times 10^{10}\,\text{Pa}$, $\rho = 2{\cdot}7 \times 10^3\,\text{kg/m}^3$ and $\nu = 0{\cdot}3$ has a frequency of 2·0288 kHz. The fundamental frequency for a corresponding simply supported S_S–S_L panel is 1·4478 kHz.

4.2. PARAMETRIC STUDIES

The influences of the length ratio, L/a, on the frequency parameters are presented in Figures 2–5 with each figure individually representing each of the four boundary conditions considered. It is evident that all the frequency modes decrease as the L/a ratio is increased. This is reasonable and intuitively correct as a length increase will generally result in decreased stiffness. Also, as the length ratio is increased, the frequencies of the first five modes tend to converge. For the panel configuration considered, the fundamental mode for this range of results corresponds to mode $(m, n) = (1, 2)$ for all four boundary conditions. No curve veering, see Kuttler and Sigillito [28] and Perkins and Mote [29], is observed. However, eigenvalue crossings are observed for the C_S–C_L and S_S–C_L cases where mode $(m, n) = (1, 1)$ starts off as the third mode and, as the length ratio is increased, crosses the profiles of modes $(m, n) = (1, 4)$ and $(1, 5)$ to become the fourth and subsequently the fifth mode. Further, it is observed that the boundary conditions considered do not affect the qualitative nature of the results presented in Figures 2–5. This should be

TABLE 1

Convergence characteristics and comparison of frequency parameter, $f = \omega b\sqrt{\rho h/A_{11}}$, with results generated from MSC/NASTRAN for a conical panel of parameters $\alpha = 20^\circ$, $\beta = 60^\circ$, $h = 0{\cdot}015a$, $L = 20a$, $v = 0{\cdot}3$ and axial wave number $m = 1$

Boundary conditions	Grid points	Circumferential wave number, n					
		2	3	4	5	6	7
C_S–C_L	7	0·0922(−3·34%)	0·1174(−7·40%)	0·1512(−4·08%)	0·2126(−9·99%)	0·2983(−18·12%)	0·4027(−24·83%)
	9	0·0903(−1·19%)	0·1115(−2·01%)	0·1493(−2·78%)	0·2003(−3·60%)	0·2600(−2·95%)	0·3380(−4·79%)
	11	0·0898(−0·61%)	0·1103(−0·92%)	0·1473(−1·40%)	0·1966(−1·72%)	0·2594(−2·72%)	0·3316(−2·79%)
	13	0·0895(−0·33%)	0·1099(−0·50%)	0·1464(−0·76%)	0·1956(−1·17%)	0·2564(−1·55%)	0·3294(−2·12%)
	15	0·0894(−0·17%)	0·1096(−0·27%)	0·1460(−0·46%)	0·1948(−0·75%)	0·2554(−1·14%)	0·3277(−1·59%)
	NASTRAN	0·0892	0·1093	0·1453	0·1933	0·2525	0·3226
S_S–C_L	7	0·0922(−3·29%)	0·1174(−7·44%)	0·1510(−3·92%)	0·2125(−9·92%)	0·2982(−18·08%)	0·4026(−24·81%)
	9	0·0902(−1·14%)	0·1115(−2·01%)	0·1493(−2·77%)	0·2003(−3·59%)	0·2599(−2·94%)	0·3380(−4·78%)
	11	0·0898(−0·61%)	0·1103(−0·92%)	0·1473(−1·40%)	0·1966(−1·72%)	0·2594(−2·72%)	0·3315(−2·79%)
	13	0·0895(−0·33%)	0·1099(−0·50%)	0·1464(−0·76%)	0·1956(−1·17%)	0·2564(−1·55%)	0·3294(−2·12%)
	15	0·0894(−0·27%)	0·1096(−0·27%)	0·1460(−0·46%)	0·1948(−0·75%)	0·2554(−1·14%)	0·3277(−1·59%)
	NASTRAN	0·0892	0·1093	0·1453	0·1933	0·2525	0·3226
C_S–S_L	7	0·0648(1·11%)	0·0840(8·40%)	0·1340(−2·95%)	0·2059(−14·56%)	0·2950(−22·89%)	0·4006(−28·85%)
	9	0·0623(4·90%)	0·0916(0·08%)	0·1269(2·51%)	0·1768(1·64%)	0·2451(−2·09%)	0·3288(−5·75%)
	11	0·0632(3·53%)	0·0903(1·44%)	0·1303(−0·16%)	0·1793(0·21%)	0·2388(0·52%)	0·3119(−0·30%)
	13	0·0636(2·90%)	0·0908(0·98%)	0·1297(0·34%)	0·1805(−0·43%)	0·2417(−0·69%)	0·3132(−0·73%)
	15	0·0638(2·65%)	0·0909(0·83%)	0·1299(0·16%)	0·1801(−0·24%)	0·2419(−0·76%)	0·3147(−1·22%)
	NASTRAN	0·0655	0·0917	0·1301	0·1797	0·2401	0·3109
S_S–S_L	7	0·0642(1·99%)	0·0842(8·14%)	0·1341(−3·03%)	0·2059(−14·58%)	0·2950(−22·89%)	0·4006(−28·85%)
	9	0·0622(5·06%)	0·0916(0·11%)	0·1269(2·51%)	0·1768(1·61%)	0·2451(−2·10%)	0·3289(−5·76%)
	11	0·0632(3·55%)	0·0903(1·44%)	0·1303(−0·16%)	0·1793(0·22%)	0·2389(0·51%)	0·3119(−0·30%)
	13	0·0636(2·91%)	0·0908(0·97%)	0·1297(0·34%)	0·1805(−0·43%)	0·2417(−0·69%)	0·3132(−0·73%)
	15	0·0638(2·65%)	0·0909(0·83%)	0·1299(0·17%)	0·1801(−0·24%)	0·2419(−0·76%)	0·3147(−1·22%)
	NASTRAN	0·0655	0·0917	0·1301	0·1797	0·2401	0·3109

Note: Numbers in parentheses denote discrepancies against FEM results.

TABLE 2

Convergence characteristics and comparison of frequency parameter, $f = \omega b\sqrt{\rho h/A_{11}}$, *with results generated from MSC/NASTRAN for a conical panel of parameters* $\beta = 60^\circ$, $h = 0{\cdot}02a$, $L = 25a$, $v = 0{\cdot}3$, *and mode* $(m, n) = (1, 2)$

Boundary conditions	Grid points	Vertex angle, α			
		10°	20°	30°	40°
C_S–C_L	7	0·0908(−7·26%)	0·0963(−3·12%)	0·1138(−3·24%)	0·1252(2·94%)
	9	0·0862(−1·78%)	0·0947(−1·40%)	0·1115(−1·17%)	0·1253(2·87%)
	11	0·0855(−0·91%)	0·0941(−0·71%)	0·1108(−0·57%)	0·1245(3·50%)
	13	0·0852(−0·56%)	0·0938(−0·42%)	0·1105(−0·30%)	0·1242(3·74%)
	15	0·0850(−0·36%)	0·0937(−0·25%)	0·1104(−0·15%)	0·1240(3·87%)
	NASTRAN	0·0847	0·0934	0·1102	0·1290

Note: Numbers in parentheses denote discrepancies against FEM results.

TABLE 3

Convergence characteristics and comparison of frequency parameter, $f = \omega b\sqrt{\rho h/A_{11}}$, *with results generated from MSC/NASTRAN for a conical panel of parameters* $\alpha = 30^\circ$, $h = 0{\cdot}02a$, $L = 20a$, $v = 0{\cdot}3$, *and mode* $(m, n) = (1, 4)$

Boundary conditions	Grid points	Subtended angle, β			
		15°	30°	45°	60°
C_S–C_L	7	2·0326(−43·79%)	0·5151(−24·91%)	0·2435(−8·11%)	0·1708(−5·00%)
	9	1·6315(−15·41%)	0·4321(−4·80%)	0·2345(−4·09%)	0·1664(−2·28%)
	11	1·5006(−6·15%)	0·4244(−2·93%)	0·2299(−2·05%)	0·1647(−1·26%)
	13	1·4645(−3·60%)	0·4215(−2·22%)	0·2283(−1·33%)	0·1639(−0·72%)
	15	1·4619(−3·42%)	0·4191(−1·65%)	0·2273(−0·91%)	0·1634(−0·41%)
	NASTRAN	1·4136	0·4123	0·2253	0·1627

Note: Numbers in parentheses denote discrepancies against FEM results.

expected as these results, in their corresponding sets, have correspondingly similar mode shape forms.

In Figures 6–9, the influences of the vertex angle, α, on the frequency parameters are examined, with again each figure individually representing each of the four boundary conditions considered. With the general exception of mode $(m, n) = (1, 1)$, the frequencies associated with all other modes decrease with increased vertex angles. For mode $(m, n) = (1, 1)$, the frequencies first increase gradually until α is in the range of 35–40° before decreasing to join the other frequency profiles in a convergent manner as α is increased further. Again, no eigenvalue veering is observed here. Crossings are, however, observed with mode $(m, n) = (1, 1)$ being especially obvious where it starts as the fundamental mode but with subsequent crossings invariably become the highest of the five modes being plotted. Further, there are some "minor" crossings in the C_S–C_L and S_S–C_L cases involving mode $(m, n) = (1, 2)$ when the frequencies begin to converge as α is increased. In Figures 6–9, we also observe that the mode shape of the fundamental frequency varies as α increases. Taking Figure 7 as an example, as α is gradually increased, the fundamental frequency is

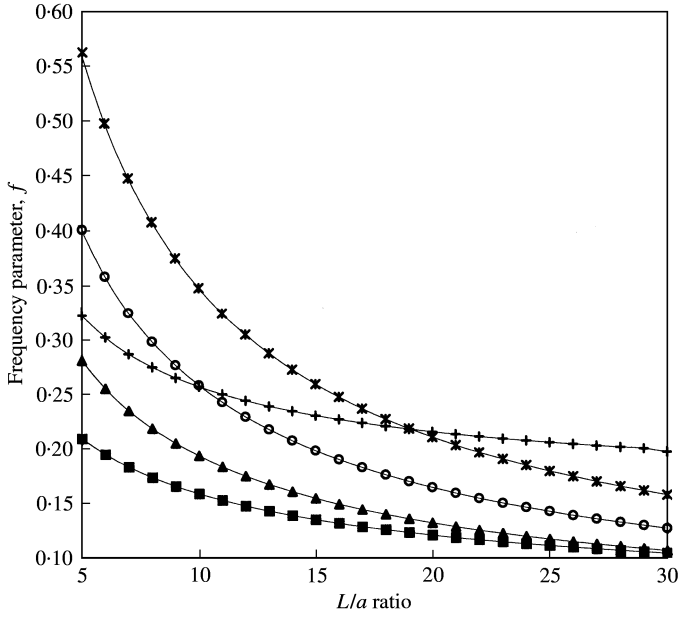

Figure 2. Frequency parameter, $f = \omega b\sqrt{\rho h/A_{11}}$, against length ratio, L/a, for a conical panel of parameters $\alpha = 30^\circ$, $\beta = 60^\circ$, $h = 0{\cdot}02a$, $v = 0{\cdot}3$ and $m = 1$ (C_S–C_L): —+—, $n = 1$; —■—, $n = 2$; —▲—, $n = 3$; —●—, $n = 4$; —✱—, $n = 5$.

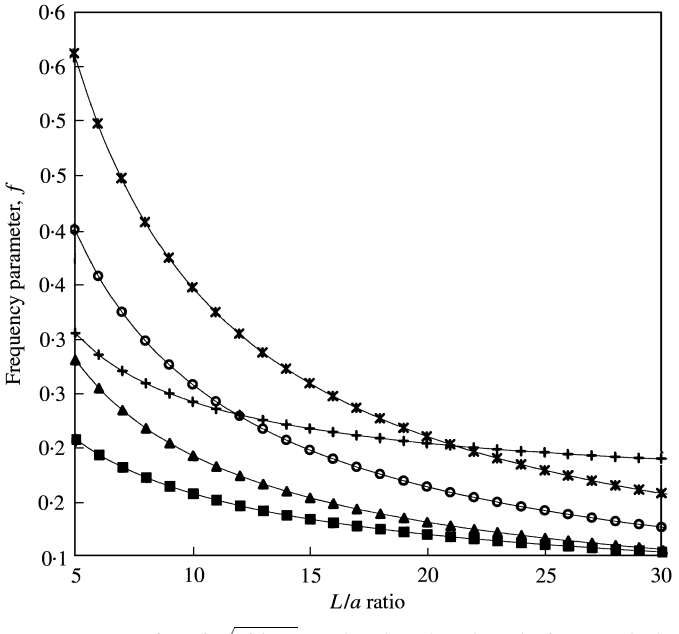

Figure 3. Frequency parameter, $f = \omega b\sqrt{\rho h/A_{11}}$, against length ratio, L/a, for a conical panel of parameters $\alpha = 30^\circ$, $\beta = 60^\circ$, $h = 0{\cdot}02a$, $v = 0{\cdot}3$ and $m = 1$ (S_S–C_L): —+—, $n = 1$; —■—, $n = 2$; —▲—, $n = 3$; —●—, $n = 4$; —✱—, $n = 5$.

first associated with mode $(m, n) = (1, 1)$, followed by mode $(m, n) = (1, 2)$ and finally with mode $(m, n) = (1, 3)$. With the exception when α is small, the fundamental frequency generally decreases with increased α, regardless of which mode shape it is associated with.

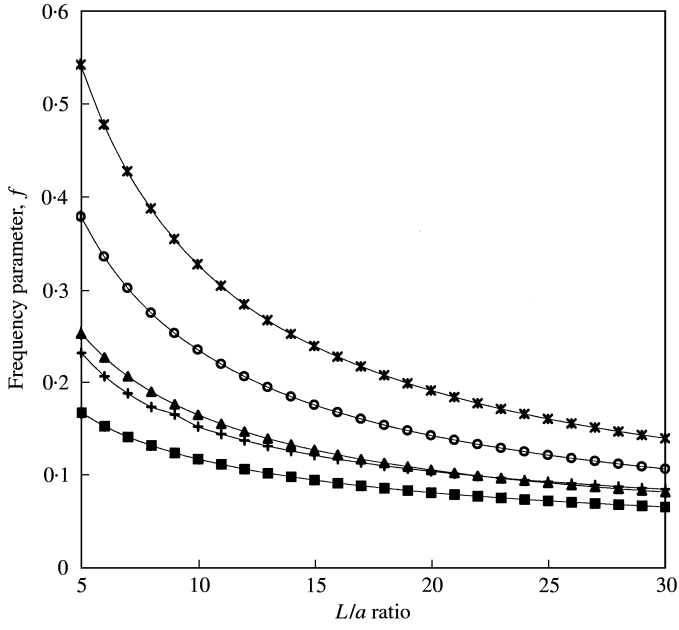

Figure 4. Frequency parameter, $f = \omega b\sqrt{\rho h/A_{11}}$, against length ratio, L/a, for a conical panel of parameters $\alpha = 30^\circ$, $\beta = 60^\circ$, $h = 0{\cdot}02a$, $v = 0{\cdot}3$ and $m = 1$ (C_S–S_L): —+—, $n = 1$; —■—, $n = 2$; —▲—, $n = 3$; —●—, $n = 4$; —✱—, $n = 5$.

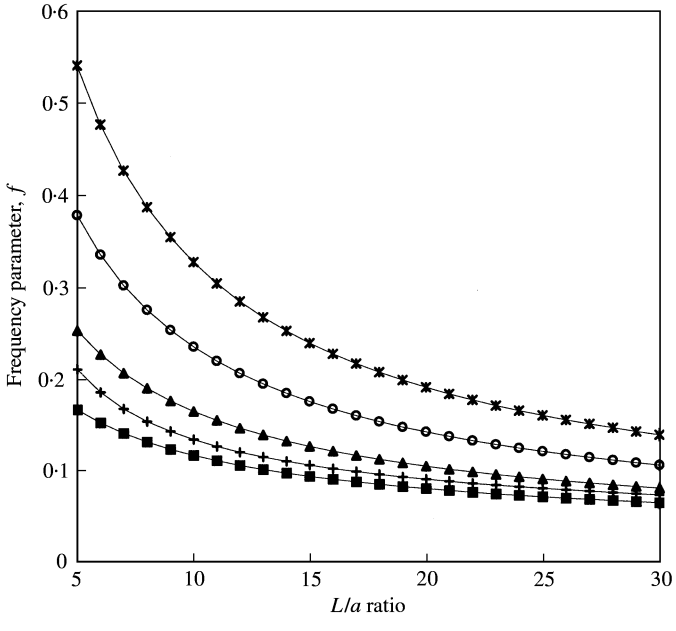

Figure 5. Frequency parameter, $f = \omega b\sqrt{\rho h/A_{11}}$, against length ratio, L/a, for a conical panel of parameters $\alpha = 30^\circ$, $\beta = 60^\circ$, $h = 0{\cdot}02a$, $v = 0{\cdot}3$ and $m = 1$ (S_S–S_L): —+—, $n = 1$; —■—, $n = 2$; —▲—, $n = 3$; —●—, $n = 4$; —✱—, $n = 5$.

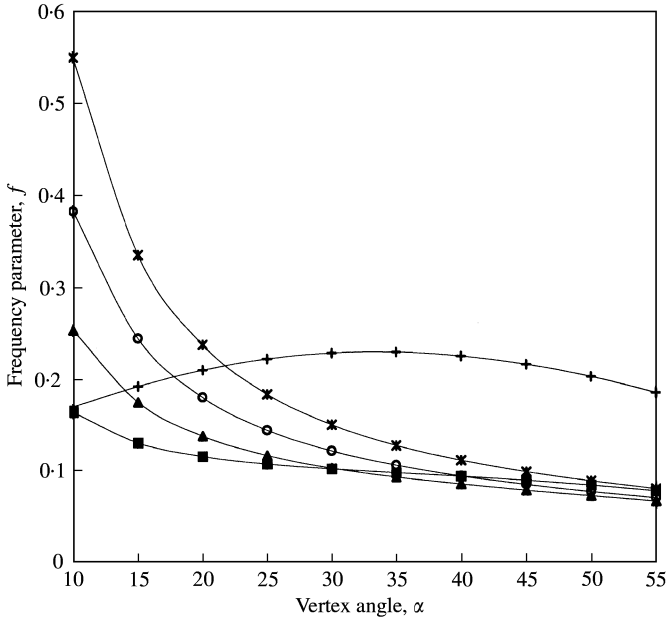

Figure 6. Frequency parameter, $f = \omega b\sqrt{\rho h/A_{11}}$, against vertex angle, α, for a conical panel of parameters $L = 15a$, $\beta = 60^\circ$, $h = 0{\cdot}01a$, $v = 0{\cdot}3$ and $m = 1$ (C_S–C_L): —+—, $n = 1$; —■—, $n = 2$; —▲—, $n = 3$; —●—, $n = 4$; —✱—, $n = 5$.

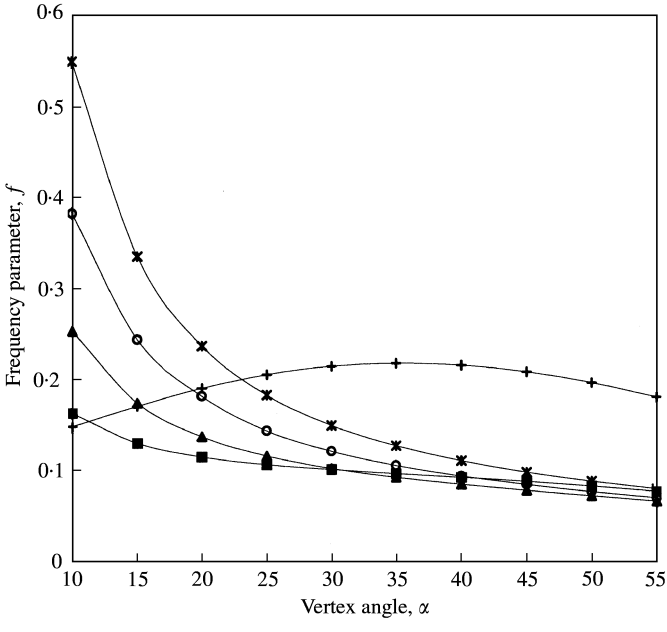

Figure 7. Frequency parameter, $f = \omega b\sqrt{\rho h/A_{11}}$, against vertex angle, α, for a conical panel of parameters $L = 15a$, $\beta = 60^\circ$, $h = 0{\cdot}01a$, $v = 0{\cdot}3$ and $m = 1$ (S_S–C_L): —+—, $n = 1$; —■—, $n = 2$; —▲—, $n = 3$; —●—, $n = 4$; —✱—, $n = 5$.

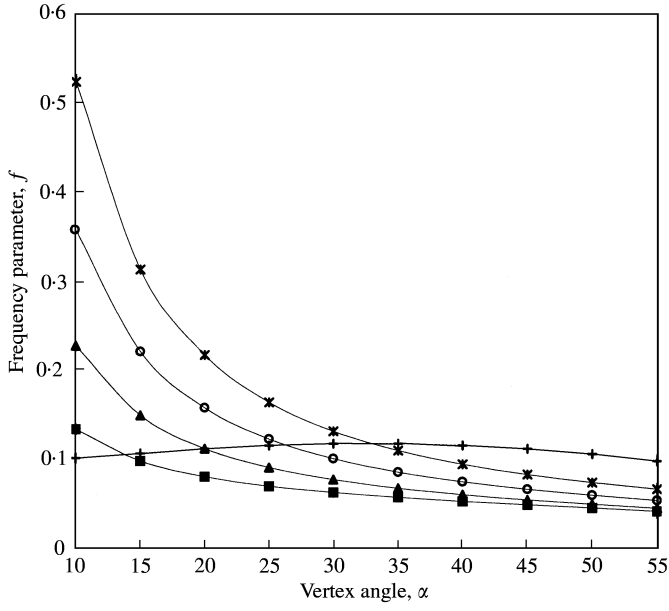

Figure 8. Frequency parameter, $f = \omega b\sqrt{\rho h/A_{11}}$, against vertex angle, α, for a conical panel of parameters $L = 15a$, $\beta = 60^\circ$, $h = 0{\cdot}01a$, $v = 0{\cdot}3$ and $m = 1$ (C_S–S_L): —+—, $n = 1$; —■—, $n = 2$; —▲—, $n = 3$; —●—, $n = 4$; —✱—, $n = 5$.

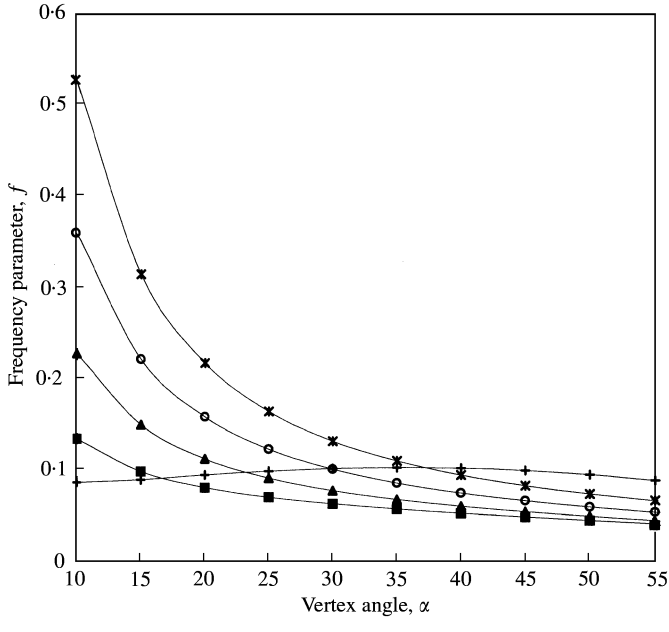

Figure 9. Frequency parameter, $f = \omega b\sqrt{\rho h/A_{11}}$, against vertex angle, α, for a conical panel of parameters $L = 15a$, $\beta = 60^\circ$, $h = 0{\cdot}01a$, $v = 0{\cdot}3$ and $m = 1$ (S_S–S_L): —+—, $n = 1$; —■—, $n = 2$; —▲—, $n = 3$; —●—, $n = 4$; —✱—, $n = 5$.

Figures 10–13 examine the influences of the subtended angle, β, on the frequency parameters corresponding to the four boundary conditions considered. It is observed that of the five modes presented here, the frequencies associated with mode $(m, n) = (1, 1)$

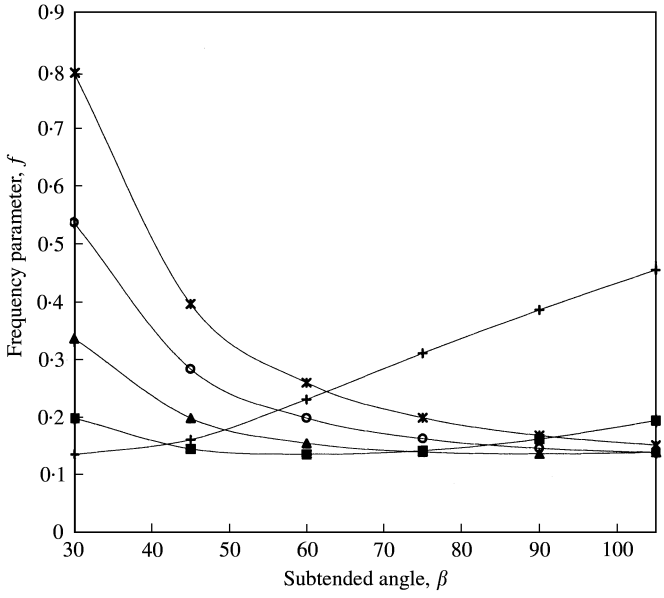

Figure 10. Frequency parameter, $f = \omega b\sqrt{\rho h/A_{11}}$, against subtended angle, β, for a conical panel of parameters $L = 15a$, $\alpha = 30^\circ$, $h = 0{\cdot}02a$, $v = 0{\cdot}3$ and $m = 1$ (C_S–C_L): —+—, $n = 1$; —■—, $n = 2$; —▲—, $n = 3$; —●—, $n = 4$; —✱—, $n = 5$.

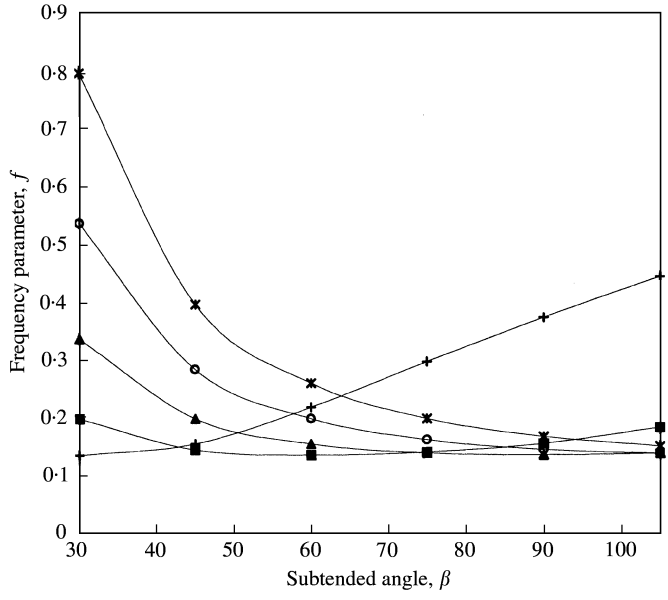

Figure 11. Frequency parameter, $f = \omega b\sqrt{\rho h/A_{11}}$, against subtended angle, β, for a conical panel of parameters $L = 15a$, $\alpha = 30^\circ$, $h = 0{\cdot}02a$, $v = 0{\cdot}3$ and $m = 1$ (S_S–C_L): —+—, $n = 1$; —■—, $n = 2$; —▲—, $n = 3$; —●—, $n = 4$; —✱—, $n = 5$.

increases with increased β, and the frequencies associated with mode $(m, n) = (1, 2)$ first decrease but there comes a turning point at which the frequencies begin to increase indefinitely. Eigenvalue crossings associated with the frequencies of these two modes

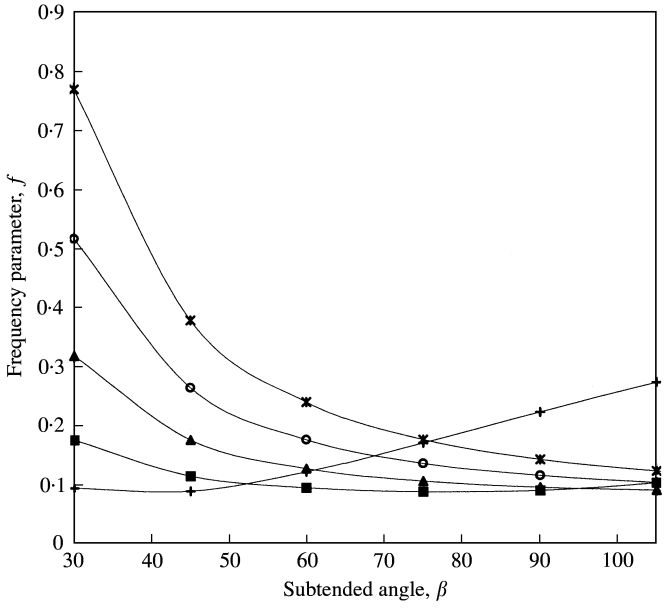

Figure 12. Frequency parameter, $f = \omega b\sqrt{\rho h/A_{11}}$, against subtended angle, β, for a conical panel of parameters $L = 15a$, $\alpha = 30°$, $h = 0{\cdot}02a$, $v = 0{\cdot}3$ and $m = 1$ (C_S–S_L): —+—, $n = 1$; —■—, $n = 2$; —▲—, $n = 3$; —●—, $n = 4$; —✱—, $n = 5$.

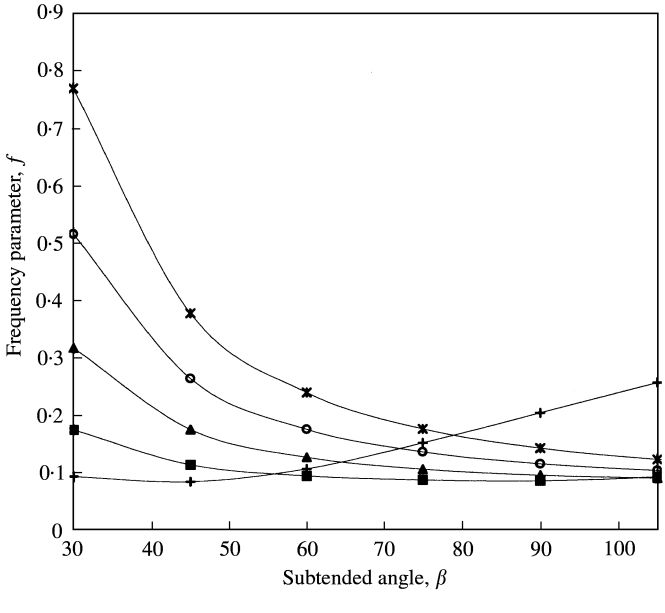

Figure 13. Frequency parameter, $f = \omega b\sqrt{\rho h/A_{11}}$, against subtended angle, β, for a conical panel of parameters $L = 15a$, $\alpha = 30°$, $h = 0{\cdot}02a$, $v = 0{\cdot}3$ and $m = 1$ (S_S–S_L): —+—, $n = 1$; —■—, $n = 2$; —▲—, $n = 3$; —●—, $n = 4$; —✱—, $n = 5$.

increasing with β are observed throughout. The other three modes seem to converge as β is increased. Here again, no eigenvalue veering is observed. As in Figures 6–9, we observe in Figures 10–13 that the mode shape of the fundamental frequency varies as β increases. It is

observed in these plots that as β is gradually increased, the fundamental frequency is first associated with mode $(m, n) = (1, 1)$, followed by mode $(m, n) = (1, 2)$ and finally with mode $(m, n) = (1, 3)$. If we disregard the associated mode shapes, the fundamental frequency generally varies little with β.

Also, as in Figures 2–5, the effects of the boundary conditions considered, for Figures 6–9 and for Figures 10–13, also do not result in any qualitative differences. Again, this is expected as these results, in their corresponding sets, have correspondingly similar mode shape forms.

5. CONCLUSIONS

An improved generalized differential quadrature (GDQ) method has been presented for the free vibration analysis of truncated conical panels. Detailed convergence and comparison studies conducted demonstrate the accuracy and stability of the proposed methodology for this geometry. Results were presented for four boundary condition types and parametric studies into the effects of the vertex and subtended angles on the frequency parameters were also examined in detail. No curve veerings associated with the variation of the natural frequencies with the physical shell parameters were observed.

REFERENCES

1. C. H. Chang 1981 *The Shock and Vibration Digest* **13**, 9–17. Vibration of conical shells.
2. H. Saunders, E. J. Wisniewski and P. R. Paslay 1960 *Journal of the Acoustical Society of America* **32**, 765–772. Vibration of conical shells.
3. J. E. Goldberg, J. L. Bogdanoff and L. Marcus 1960 *Journal of the Acoustic Society of America* **32**, 738–742. On the calculation of the axisymmetric modes and frequencies of conical shells.
4. A. Kalnins 1964 *Journal of the Acoustical Society of America* **36**, 1355–1363. Free vibration of rotationally symmetric shells.
5. H. Garnet and J. Kemper 1964 *American Society of Mechanical Engineers Journal of Applied Mechanics* **31**, 458–466. Axisymmetric free vibration of conical shells.
6. C. C. Siu and C. W. Bert 1970 *Journal of the Acoustic Society of America* **47**, 943–945. Free vibration analysis of sandwich conical shells with free edges.
7. T. Irie, G. Yamada and Y. Kaneko 1982 *Journal of Sound and Vibration* **82**, 83–94. Free vibration of a conical shell with variable thickness.
8. T. Irie, G. Yamada and Y. Kaneko 1982 *Journal of Sound and Vibration* **92**, 447–453. Natural frequencies of truncated conical shells.
9. L. Tong 1993 *International Journal of Engineering Science* **31**, 719–733. Free vibration of orthotropic conical shells.
10. L. Tong 1993 *International Journal of Mechanical Sciences* **35**, 47–61. Free vibration of composite laminated conical shells.
11. C. Shu 1996 *International Journal of Mechanical Sciences* **38**, 935–949. An efficient approach for free vibration analysis of conical shells.
12. Y. L. Wang, R. H. Liu and X. W. Wang 1999 *Journal of Sound and Vibration* **224**, 387–394. Free vibration analysis of truncated conical shells by the differential quadrature method.
13. J. N. Rossetos and R. F. Parisse 1969 *American Society of Mechanical Engineers Journal of Applied Mechanics* **36**, 271–276. The dynamic response of cylindrical and conical panels.
14. D. G. Ashwell and R. Gallagher 1976 *Finite Element Thin Shell Analysis*. New York: John Wiley.
15. D. G. Ashwell and R. Gallagher 1976 *Finite Element for Thin Shell and Curve Members*. New York: John Wiley.
16. D. Teichmann 1985 *American Institute of Aeronautics and Astronautics Journal* **23**, 1634–1637. An approximation of the lowest eigenfrequencies and buckling loads of cylindrical and conical shell panels under initial stress.

17. R. S. Srinivasan and P. A. Krishnan 1987 *Journal of Sound and Vibration* **117**, 153–160. Free vibration of conical shell panels.
18. Y. K. Cheung, W. Y. Li and L. G. Tham 1989 *Journal of Sound and Vibration* **128**, 411–422. Free vibration analysis of singly curved shell by spline finite strip method.
19. Y. M. Grigorenko, N. N. Kryukov and O. M. Shutovsky 1990 *Dopovidi Akademii Nauk Ukrainskoi RSR Seriya A—Fiziko-Matematichni ta Technichni Nauki* **10**, 37–41. Solution of 2-dimensional problems on deformation of non-shallow conical panels on the spline-approximation basis.
20. K. M. Liew and M. K. Lim 1995 *Engineering Structures* **17**, 63–70. Vibratory behaviour of shallow conical shells by a global Ritz formulation.
21. C. W. Lim and K. M. Liew 1995 *International Journal of Solids and Structures* **33**, 451–468. Vibration of shallow conical shells with shear flexibility: a first order theory.
22. C. W. Lim and S. Kitipornchai 1999 *Journal of Sound and Vibration* **219**, 813–835. Effects of subtended and vertex angles on the free vibration of open conical shell panels: a conical co-ordinate approach.
23. N. S. Bardell, J. M. Dunsdon and R. S. Langley 1998 *Journal of Sound and Vibration* **217**, 297–320. A h-p finite element analysis of open conical sandwich panels and conical sandwich frusta.
24. C. W. Bert and M. Malik 1996 *Applied Mechanics Reviews* **49**, 1–28. Differential quadrature method in computational mechanics: a review.
25. R. H. Gutierrez, P. A. A. Laura and R. E. Rossi 1994 *Ocean Engineering* **21**, 57–66. The method of differential quadrature and its application to the approximate solution of ocean engineering problems.
26. K. Y. Lam and H. Li 1997 *International Journal of Solids and Structures* **34**, 2183–2197. Vibration analysis of a rotating truncated circular conical shell.
27. A. E. H. Love 1927 *A Treatise on the Mathematical Theory of Elasticity*. New York: Cambridge University Press; fourth edition.
28. J. R. Kuttler and V. G. Sigillito 1981 *Journal of Sound and Vibration* **75**, 585–588. On curve veering.
29. N. C. Perkins and C. D. Mote 1986 *Journal of Sound and Vibration* **106**, 451–463. Comments on curve veering in eigenvalue problems.